Cite this: DOI: 10.1039/c0xx00000x

www.rsc.org/xxxxxx

ARTICLE TYPE

In situ surface hydrogenation synthesis of Ti^{3+} self−doped TiO_2 with enhanced visible light photoactivity

Junchao Huo, Yanjie Hu*, Hao Jiang and Chunzhong Li*

Received (in XXX, XXX) Xth XXXXXXXXX 20XX, Accepted Xth XXXXXXXXX 20XX

DOI: 10.1039/b000000x

A novel one−step vapor−fed aerosol flame synthetic process (VAFS) has been developed to prepare Ti^{3+} self−doped titanium dioxide (TiO_2). The freshly formed TiO_2 was in situ surface hydrogenated during the condensation stage by introducing of H_2 above the flame and Ti^{3+} ions were created near the surface of TiO_2. The relative content of Ti^{3+} ions near the surface of TiO_2 is estimated to be 8%. Because of the high absorption of visible light and suppression of charge recombination，the photocurrent density and decomposition of MB under visible light irradiation were remarkably enhanced. This study demonstrates a simple and potential method to produce Ti^{3+} self−doped TiO_2 with effective photoactivity in visible light.

Introduction

Owing to its chemical stability, earth abundance, low toxicity and excellent photoactivity,[1] TiO_2 has got much attention for its promising application as an active material in photovoltaics,[2] splitting of water,[3] and photocatalysts.[4] However, the application of TiO_2 is greatly hindered by ineffective utilization of visible light[5] (43% of the total solar energy), which results from the wide band gap (3.2 eV).[6] Therefore various strategies have been designed to modify the properties of TiO_2, aiming to narrow the band gap, such as coupling TiO_2 with a narrow band gap metal oxide,[7] metal or nonmetal ion doping,[8] co−doping with different kinds of ions and surface sensitization using quantum dot or organic dyes.[9]

Recently, reduced TiO_2 contains Ti^{3+} ions has been designed as an effective and environment friendly strategy to improve visible light photoactivity.[10] Ti^{3+} self−doped TiO_2 synthesized by a liquid process has been reported,[11] and the resulting blue sample showed effective performance in water splitting under visible light. Chen et al.[12] prepared hydrogenated TiO_2 nanocrystals by introducing a surface disorder structure, extending the light absorption to near infrared range (~1200 nm), and the samples exhibited significant photocatalytic activity in visible light. Wang et al.[13] reported that the light absorption and water splitting ability of TiO_2 nanowire arrays were significantly enhanced by hydrogenation. Several approaches have been reported to produce Ti^{3+} self−doped TiO_2,[14,15] such as hydrogen thermal treatment,[16] high energy particle bombardment[17,18] and thermal annealing[19] under oxygen depleted condition etc. Although these methods have their own advantages, they are limited by high cost, complicated procedures and little scale production. Thus, there is an urgent need to develop a simple and large scale synthetic strategy to prepare Ti^{3+} self−doped TiO_2 with efficient photoactivity in visible light.

Flame synthesis[20] approach is wildly used in the production of oxide semiconductor nanoparticles such as TiO_2,[21] SiO_2[22] and so on. This method has many advantages, such as usable in large quantities, being continuous and requiring no posttreatment. Nowadays, various non−stoichiometry semiconductor oxides and nonoxidation compounds have been synthesized by modified flame synthesis equipments. For example, single crystalline SnO nanoplatelets were rapidly synthesized via reducing atmosphere flame spray pyrolysis (RAFSP) without the assistance of catalyst and surfactant.[23] Oxygen deficient titania nanoparticles has been synthesized by a diffusion flame reactor with an oxygen deficit environment in the reaction section.[24] Using different ration of fuel and air， Strobel and Pratsinis[25] prepared maghemite, magnetite, and wustite nanoparticles. Stark et al.[26] created reducing flame technology for the synthesis of non−agglomerated Co@C, Fe_3C@C core−shell nanomagnets with high stability and excellent saturation magnetization. Air stable Co_3Fe_7−$CoFe_2O_4$ nanoparticles[27] have been synthesized under strong reducing atmosphere by a one−step flame spray pyrolysis process.

In this work, a novel one−step route has been developed to synthesized Ti^{3+} self−doped TiO_2 by simply introducing H_2 above the flame where the TiO_2 nanoparticles were just formed. The freshly formed TiO_2 nanoparticles were surface hydrogenated at the condensation stage. In addition, owing to the high adsorption of visible light and suppression of charge recombination, the photocurrent density and decomposition of MB under visible light irradiation were remarkably enhanced.

Experimental Section

Ti^{3+} self–doped TiO_2 nanoparticles synthesis.

Ti^{3+} self–doped TiO_2 nanoparticles were prepared by a modified vapor–fed aerosol flame synthesis (VAFS) equipment (shown in Fig. S1, ESI†). Schematically, it consists of three parts, parameters control section, chemical reaction section and products collection section. The reaction part contains a H_2/O_2 co–flow diffusion flame nozzle and a stainless steel metal torus pipe ring. The nozzle is fabricated by three concentric metal tubes, the diameters of the tubes are 10.0, 6.0, and 3.0 mm, respectively. The pipe ring (D=10 mm) is positioned just above the nozzle for the hydrogenation of TiO_2, with a height of 15cm. There are 16 openings (D=1 mm) uniformly distribute on the ring from up–centerline.

The preparing of Ti^{3+} self–doped TiO_2 nanoparticles was performed by two steps: synthesis TiO_2 nanoparticles and hydrogenation of TiO_2 nanoparticles. Titanium tetrachloride ($TiCl_4$) vapor was fed into the coflow diffusion flame, supplied by hydrogen (inner annulus) and oxygen (outer annulus), to synthesize TiO_2 nanoparticles. A steam of nitrogen through a gas washing bottle with liquid $TiCl_4$ was used to carry $TiCl_4$ vapor, the temperature of liquid $TiCl_4$ was fixed at 30 °C. The $TiCl_4$ vapor carried by nitrogen stream was delivered into the central tube of the flame nozzle, together with a diluting nitrogen gas. The flow rates of hydrogen and oxygen were 380 L/h and 190 L/h, respectively. Controlling the ratio of fuel to oxygen to be 1 was the key point of this process, which was beneficial to the hydrogenation of TiO_2 nanoparticles. Hydrogenation of TiO_2 nanoparticles was achieved by introducing a flow rate of 760 L/h of hydrogen above the flame in which TiO_2 nanoparticles were formed. The freshly formed TiO_2 reacted with H_2 molecules at a high temperature of about 700 °C supplied by the flame, then formed Ti^{3+} self–doped TiO_2 nanoparticles. All gases flow rates in the process were monitored by rotameters. Glass fiber filters were used to collect the products, aiding by a vacuum pump.

The amount of $TiCl_4$ vapor can be calculated by the statured vapor pressure approximately, supposing that $TiCl_4$ vapor is statured. The saturation partial pressure of $TiCl_4$ vapor can be calculated by equation

$$Log_{10}(P) = 4.84969 - \frac{1990.235}{T+2} \tag{1}$$

in which P is saturation partial pressure of $TiCl_4$ vapor, T is the temperature of glass flask (303K). The velocity of $TiCl_4$ vapor supplied was calculated to be about 0.01–0.2 mol/h, and the yield could be 1–16 g/h, theoretically. In our experiment, 40 L/h of carrier gas was used, and the yield was calculated to be about 3.2 g/h.

Characterization and Measurements

X–ray diffraction (XRD; Rigaku D/max 2550) was used to characterize the crystallinity of the samples. The morphologies of Ti^{3+} self–doped TiO_2 were investigated using scanning electron microscopy (SEM; Hitachi S–4800), high–resolution transmission electron microscopy (TEM; JEM–2010). UV–vis spectrums were carried out by an UV–vis spectrophotometer (Cary–500 spectrometer, Varian Ltd.). An X–ray photoelectron spectrometer (ESCALAB MK II) was used to measure the the X–ray photoelectron spectra (XPS) using the reference of C 1s (284.6 eV), with the excitation source of Mg Ka (1253.6 eV) X–rays. The electron paramagnetic resonance (EPR) spectra were carried out via a Bruker EPR ELEXSYS 500 spectrometer.

Photocurrent measurements

An uniform slurry was first prepared by dispersing Ti^{3+} self–doped TiO_2 nanoparticles (10 mg) into anhydrous ethanol (5 mL) and ultrasonically vibrating for 20 min. Then the resultant slurry was dip–coated onto a 20 × 30 mm FTO glass electrode and dried in air to eliminate ethanol. The sample of TiO_2 without hydrogenation was treated in the same way for comparison. The prepared TiO_2/FTO electrode was assembled with a platinum electrode (counter electrode) and silver chloride electrode (reference electrode) into a three-electrode cell. 0.5 mol/L Na_2SO_4 aqueous solution was employed as electrolyte. Before testing, the TiO_2/FTO electrode was immersed into the electrolyte and activated for 30 min to keep it stable. A Xe lamp (300 W) positioned 10 cm away from the working electrode was used as the light source. An ultraviolet cutoff filter was applied to cutoff the UV light (λ < 400 nm). An electrochemical workstation was employed to measure the photocurrent intensity of the samples under intermittent illumination.[28]

Photocatalytic activity measurements

The photocatalytic activity of the samples was performed by measuring the degradation of methylene blue (MB). MB is a cationic thiazine dye with a brightly blue color and is widely applied as a test model pollutant in photocatalytic process. Visible light ($\lambda \geq 400$ nm) was provided with a 300 W Xe lamp, and an ultraviolet cutoff filter was applied to cutoff the UV light. Generally, 50 mg of the nanoparticles were dispersed in 80 mL aqueous solution of MB with a concentration of 5.0×10^{-4} mol/L in a customized quartz test tube. The concentration of MB was characterized by UV–vis spectroscopy during the entire experiment. Before measurement, the suspension was first stirred for 30 min in dark to ensure the equilibrium of adsorption–desorption between photocatalysts and MB. Then the suspension was irradiated by the Xe lamp 10 cm away. During the irradiation, about 5 mL of the suspension was taken out after every 20 min intervals, and centrifuged to separate the nanoparticles. The concentration of MB in the centrifuged solution was carried out by a UV–vis spectroscopy in the range from 200 to 800 nm.

Results and Discussion

The Morphology of Ti^{3+} self–doped TiO_2 nanoparticles.

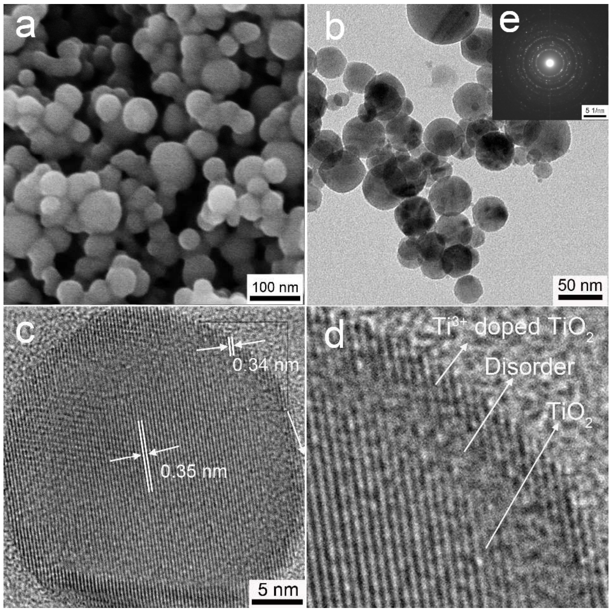

Fig. 1 (a) SEM image of Ti^{3+} self–doped TiO_2, (b) TEM image of Ti^{3+} self–doped TiO_2, (c) HRTEM image, (d) Disorder from HRTEM image, (e) The SAED pattern of Ti^{3+} self–doped TiO_2

The typical microstructure of Ti^{3+} self-doped TiO_2 samples was observed by SEM and TEM analyses. Spherical Ti^{3+} self–doped TiO_2 nanoparticles with fine dispersibility are obtained (Fig. 1a and b), the particle size is estimated to be 20–40 nm. The BET surface area of the sample is 42.3 m^2/g, and the total pore volume is 0.118 cm^3/g (Fig. S2, ESI). HRTEM image (Fig. 1c) results show that the sample has a good crystallization, a lattice spacing of 0.35 nm between the (101) planes and the framework of the highly crystalline TiO_2 can be clearly observed. However, the lattice spacing near the surface (0.34 nm) is different from that in the bulk (Fig. 1d) and an obvious disordered layer can be observed on the HRTEM image. This can be ascribed to the effect of hydrogen treating and the generation of Ti^{3+} ions near the surface. Fig. 1e shows the SAED pattern, indicating the Ti^{3+} self–doped TiO_2 nanoparticles are polycrystalline, in agreement with XRD patterns (Fig. S3, ESI). The XRD patterns suggest that the Ti^{3+} self–doped TiO_2 nanoparticles are mixture of annatase TiO_2 and rutile TiO_2. However, the anatase fraction of the sample (68.7%) is lower than that of TiO_2 without hydrogenation (91.2%). This is because of the introducing of hydrogen increases the reaction temperature above the flame, accelerates the transformation of anatase TiO_2 to rutile TiO_2.The average crystallite sizes of Ti^{3+} self-doped TiO_2 nanoparticles are calculated from the anatase (101) and rutile (110) with Scherrer equation, and are found to be 5.0 nm and 7.8 nm, respectively. The HRTEM image of Ti^{3+} self-doped TiO_2 with mixture phase is shown in Fig. S4 (ESI). The different crystal lattice can be clearly observed, indicating the sample is mixture of annatase TiO_2 and rutile TiO_2, in agreement with XRD patterns.

The blue coloration of the samples is due to the formation of Ti^{3+} ions by electron trapping at the Ti^{4+} centers, therefore the color of the obtained samples can indicate the amount of the Ti^{3+} ions in a certain extent. The color can be modified by using different amount of H_2 for hydrogenation (Fig. S5, ESI). The blue color is much darker as more hydrogenation H_2 is used when the total flow rate hydrogenation H_2 is lower than 720 L h^{-1}. Therefore the concentration of Ti^{3+} ions can be controlled by the flow rate of hydrogenation H_2. In addition, the yield and the morphology of obtained samples (Fig. S6, ESI) can both be modified by different $TiCl_4$ concentration.

XPS measurements (Fig. 2) were performed to investigate the presence and chemical states of Ti^{3+} ions in the samples. XPS reveals the elements and associated chemical bonds in the top few atomic layers of the material, for the escape depth of electrons is a few nanometers. Two peaks of Ti $2p_{3/2}$ (458.33 eV) and Ti $2p_{1/2}$ (464.33 eV) at binding energies are showed in the high resolution Ti 2p XPS spectrum of Ti^{3+} self–doped TiO_2. The peaks of Ti^{3+} self–doped TiO_2 shows a shift towards lower binding energy, indicating that the chemical environments of Ti atoms in Ti^{3+} self–doped TiO_2 are different from that in pristine TiO_2. After deconvolution, the Ti 2p peaks of Ti^{3+} self–doped TiO_2 are well divided into four peaks at 457.91 eV, 458.51 eV, 464.05 eV, 464.47 eV, represent Ti^{3+} $2p_{3/2}$, Ti^{4+} $2p_{3/2}$, Ti^{3+} $2p_{1/2}$, Ti^{4+} $2p_{1/2}$, respectively. It clearly shows the existing of Ti^{3+} ions. In the surface of hydrogen treated TiO_2, the relative content of Ti^{3+} ions is roughly calculated to be 8% by comparing the XPS peak areas of Ti^{3+} to Ti^{4+}. The presence of Ti^{3+} ions near the surface can promote the visible light adsorption and enhance the catalytic activity. [29] The O 1s XPS spectra are shown Fig. S7 (ESI), the signals centered at 529.98 eV and 531.48 eV are the typical signals of Ti–O–Ti and surface OH species, respectively. The O 1s spectra illustrates that Ti^{3+} self-doped TiO_2 has much more surface OH species.

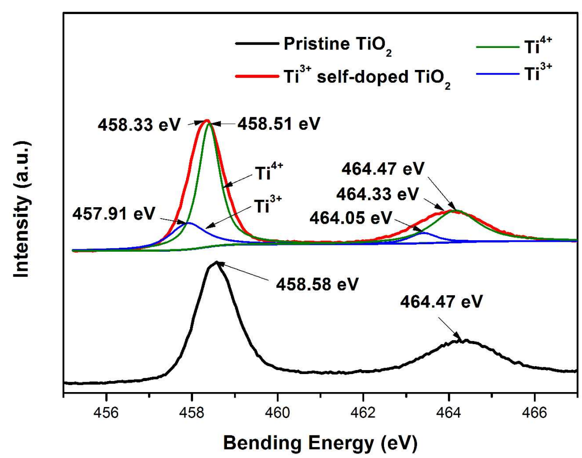

Fig. 2 High resolution XPS spectrum of Ti_{2p} of Ti^{3+} self–doped TiO_2 and pristine TiO_2

Low temperature electron paramagnetic resonance (EPR) was conducted to further identify the presence of Ti^{3+} ions. Fig. 3 shows the low temperature EPR result of the Ti^{3+} self–doped TiO_2 sample. Based on the EPR spectrum, the as synthesized Ti^{3+} self–doped TiO_2 sample gave rise to a broad signal at g = 1.999, which is the typical g values for a paramagnetic Ti^{3+} center, attributed to Ti^{3+} ions on the surface. According to previous reports, while crystalline TiO_2 is treated in vacuum or in the presence of reduced gas at a high temperature, the oxygen atoms in the lattice can be removed. Inner Ti^{3+} ions can only generate during long time and high temperature ((above 973 K) heat treatments.[30] However, we obtained a high concentration of Ti^{3+} self–doped TiO_2 by in situ treatment of H_2 at a high temperature while the freshly formed TiO_2 is on the condensation stage.

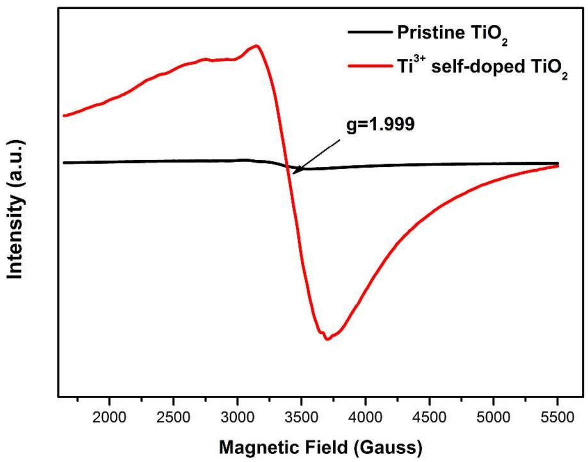

Fig. 3 EPR result of Ti^{3+} self–doped TiO_2 and pristine TiO_2

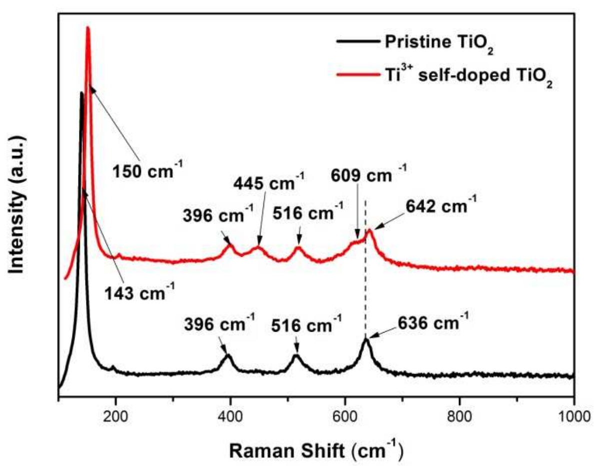

Fig. 4 Raman spectra of Ti^{3+} self–doped TiO_2 and pristine TiO_2

Raman spectra shown in Fig. 4 were performed to investigate the changes of structure on the surface of TiO_2 before and after hydrogen treated. The Raman spectrums show remarkable difference and three features can be obtained. Firstly, the diffraction peaks become weaker at 636 cm^{-1}, 516 cm^{-1}, 396 cm^{-1} and 143 cm^{-1} after hydrogen treated. Secondly, the two Eg modes at 636 cm^{-1} and 143 cm^{-1} of TiO_2 are shifted to a higher frequency to 642 cm^{-1} and 150 cm^{-1} in Ti^{3+} self–doped TiO_2, respectively. These two features demonstrate the increase of Ti^{3+} ions in the lattice structure of Ti^{3+} self–doped TiO_2. Thirdly, two diffraction peaks of 445 cm^{-1} and 609 cm^{-1} emerge in Ti^{3+} self–doped TiO_2, indicating the bigger fraction of rutile TiO_2.

The UV–vis absorption spectra were carried out to confirm the change of the color and calculate the band gap (Fig. 5). No significant response is observed in pristine TiO_2 spectrum in visible light area, caused by the wide band gap of TiO_2 (3.20 eV). However, the spectrum of Ti^{3+} self–doped TiO_2 sample exhibits a strong absorption response in the region of 400 and 1200 nm, especially when the wave length gets longer, the absorption comes much stronger. The strong absorbance in visible and infrared region is attributable to the generating of Ti^{3+} ions. A new energy level may be generated owing to the presence of Ti^{3+} ions below the conduction band, resulting in the strong response in visible region. The absorption of visible light indicates that the visible light can active the Ti^{3+} self–doped TiO_2 nanoparticles, and more electrons and holes can be generated in the photocatalytic reactions, leading to enhanced photoactivity. The calculated energy band gap of Ti^{3+} self–doped TiO_2 from the UV−vis spectrum is 3.07 eV.

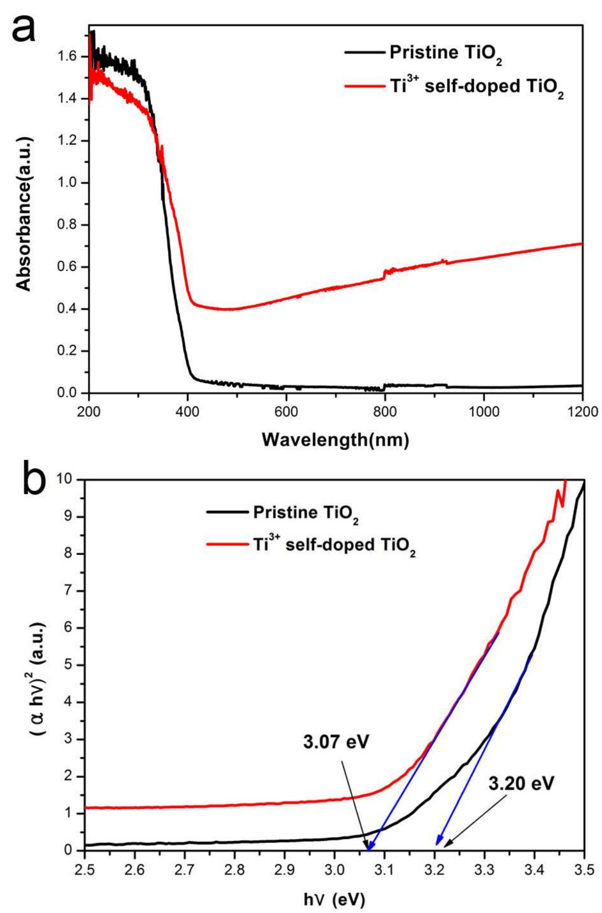

Fig. 5 (a) UV–vis spectra of Ti^{3+} self–doped TiO_2 and pristine TiO_2, (b) band gap of Ti^{3+} self–doped TiO_2 and pristine TiO_2

Photocatalytic activity

It is well known that the photocatalytic reactions are very complex, and many factors can influence the photoactivity. Among these factors, the properties of light absorption and the efficiency of photocreated electrons and holes separation are the most important. Photocatalytic degradation of MB and photoelectrical response under visible light illumination were carried out to characterize the photoactivity of the samples. The photoelectrical response of the sample was examined using a typical three–electrode method to study the separation efficiency of photogenerated electrons and holes. In comparison, the sample of pristine TiO_2 was also tested. Fig. 6 shows the photoelectrical responses of the two samples under discontinuous irradiation. Steady and prompt photocurrent generation is observed during the on and off cycles of illumination, manifesting good stability of the photocurrent for all samples. Flame made Ti^{3+} self–doped TiO_2 shows a high photocurrent density of 1090 nA/cm^2 at the time of 20 s for the first time. It is dramatically 2.55 times higher than that of pristine TiO_2 (428 nA/cm^2), indicating higher photoelectrical response and better capacity to utilize visible light for Ti^{3+} self–doped TiO_2. Moreover, the photocurrent of pristine TiO_2 disappears immediately after extinguishment of irradiation, while Ti^{3+} self–doped TiO_2 still exhibits a residual current. The relatively slower decay of the photocurrent may result from trapped charge carriers with a prolonged lifetime. This observation suggests that Ti^{3+} self–doped TiO_2 nanoparticles may be a high effective photocatalyst for degradation of organic pollutant under visible light.[31]

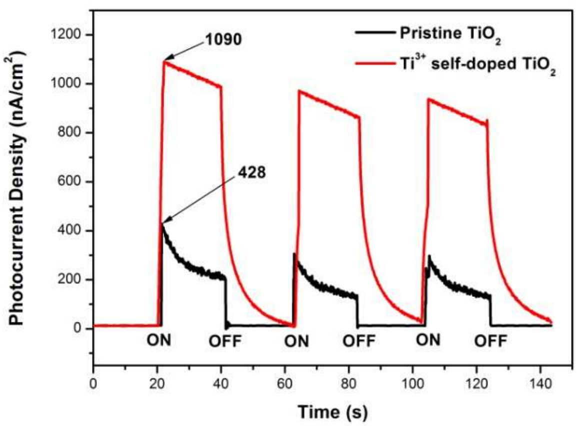

Fig. 6 Photocurrent density versus time curves of Ti^{3+} self–doped TiO_2 and pristine TiO_2

The photodegradation ability on MB solutions of Ti^{3+} self–doped TiO_2 in comparison with pristine TiO_2 and P25 is shown in Fig. 7, where t is the irradiation time, C is the MB concentration, and C_0 is MB concentration in absorption and disabsorption equilibrium before irradiation. A blank experiment in the absence of catalyst is also performed. Comparing to pristine TiO_2 and P25 nanopaticles, Ti^{3+} self–doped TiO_2 sample exhibits a significantly improvement on the decomposition of MB under visible light. The photodegradation of MB in aqueous solutions using Ti^{3+} self–doped TiO_2, pristine TiO_2 and P25 as photocatalysts with irradiation of ultraviolet light was shown in Fig. S8 (ESI). The Ti^{3+} self–doped TiO_2 sample exhibits worse photoactivity under ultraviolet light than P25 and pristine TiO_2. So the enhancement of photoactivity under visible light is mainly due to the existing of Ti^{3+} ions. As discussed above, the existing of Ti^{3+} ions can enhance the absorption of visible lights, and the Ti^{3+} species could take the effect of holes scavengers. These functions can enhance the photogenerated electrons and suppression the charge recombination, therefore enhance the photocatalytic activity.[32]

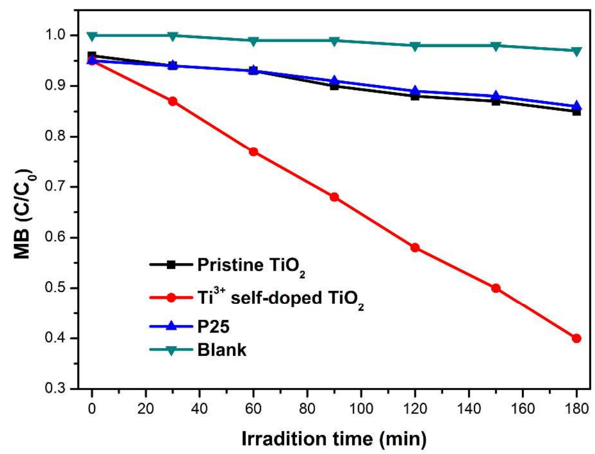

Fig. 7 Photodegradation of MB in aqueous solutions using Ti^{3+} self–doped TiO_2, pristine TiO_2 and P25 as photocatalysts with irradiation of visible light.

The influence of the defects (Ti^{3+} ions and oxygen vacancies) on the photoactivity is very complicated. Chen et al[12] reported a novel process to prepare black hydrogenated TiO_2 nanocrysyals with excellent photocatalytic performance. A disorder in the surface layers of TiO_2 was introduced, and a conduction band tail states arising from disorder that extend below the conduction band minimum was formed. However, there are still some reports on negative activity, Gu et al[33] reported the using of high-temperature hydrogenation to prepare black TiO_2 resulted in the formation of bulk defects, and the sample exhibited significantly worse photoactivity under sunlight. They proposed that the hydrogenation could be counterproductive to improve the photocatalytic activity of TiO_2 because of the formation of bulk vacancy defects. Recently there are some reports about the influence of the defect location on the photoactivity. Zhao et al [29] and Kim et al[34] argued that improving the ratio of surface to bulk defects could greatly improve the photoactivity of TiO_2. So the doping of Ti^{3+} ions in the surface of TiO_2 has the potential to enhance the photocatalytic performance.

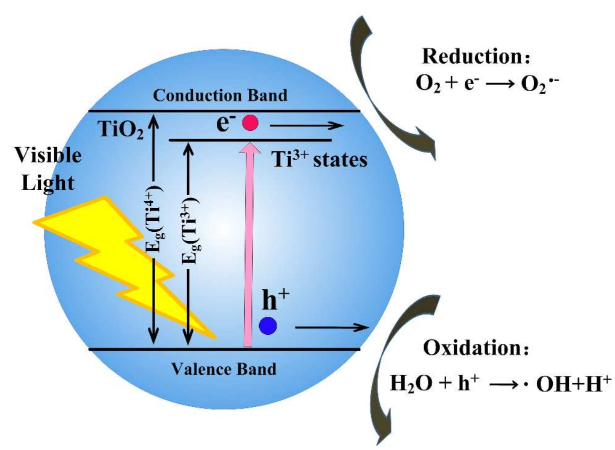

Fig. 8 Schematic of a proposed photocatalytic mechanism of Ti^{3+} self–doped TiO_2

To further investigate the effect of the introduction of Ti^{3+} ions, a schematic of a proposed photocatalytic mechanism of Ti^{3+}

self–doped TiO_2 is given (Fig. 8). The introduced Ti^{3+} ions can form sublevel states, which reduce the band gap of TiO_2, so that electrons can be photoexcited to conduction band from the valance under the irradiation of visible light. Furthermore, those Ti^{3+} ions act as the hole-traps and suppress the recombination of electrons and holes, therefore extend the charges lifetime.

Under UV irradiation, sufficient energy of light is absorbed by TiO_2 photocatalyst, an electron is excited to the conduction band, and an electron−hole pair is formed. The energy level of the conduction band depend the energy of excited electrons, excited by the lights. Under visible light irradiation, using Ti^{3+} self–doped TiO_2 as photocatalyst, almost the same process occurs, the difference is that a majority of the electrons excited by the visible light reside on the states formed by the Ti^{3+} ions. Super oxide anions are formed by the reaction of electrons and surface O_2, and act as important reluctant of organic pollutant. Strongly oxidizing •OH radicals are generated by the reaction between holes and surface water, act as necessary oxidant of the hydrocarbon.

Conclusions

In summary, a unique in situ surface hydrogenation synthetic strategy was used to prepare Ti^{3+} self–doped TiO_2 nanoparticles through a modified flame synthesis process. The sample was obtained by simply introducing H_2 above the flame in which the TiO_2 nanoparticles were formed. The freshly formed TiO_2 was surface hydrogenated during the condensation stage at a high temperature. The particle size of the Ti^{3+} self–doped TiO_2 particles is estimated to be 20–40 nm. The hydrogenation and the generation of Ti^{3+} ions make the lattice spacing near the surface different from that in the bulk, a disordered layer is formed. The concentration of the Ti^{3+} ions and the morphology of the nanoparticles can be modified by the amount of hydrogenate H_2 and precursor, respectively. The sample shows high absorption of visible light, and the energy band gap was calculated to be 3.07 eV. The relative content of Ti^{3+} ions is estimated to be 8%. The photoactivity of the sample was characterized by photoelectrical response measurement and photocatalytic degradation of MB under the irradiation of visible light. Attribute to high adsorption of visible light and suppression of charge recombination, a significantly enhancement of photocurrent density and the decomposition of MB was observed.

Acknowledgements

This work was supported by the National Natural Science Foundation of China (20925621, 21236003), the Shanghai Rising–Star Program (13QA1401100), the Basic Research Program of Shanghai (11JC1403000), the Special Projects for Nanotechnology of Shanghai (11nm0500800)，the Special Research Fund for the Doctoral Program of Higher Education of China (20110074110010, 20120074120004) and the Fundamental Research Funds for the Central Universities.

Notes and references

Key Laboratory for Ultrafine Materials of Ministry of Education, School of Materials Science and Engineering, East China University of Science and Technology, Shanghai 200237, China. Fax: +86 21 6425 0624; Tel: +86 21 6425 0494; E-mail: czli@ecust.edu.cn (Prof. C. Z. Li) and huyanjie@ecust.edu.cn (Dr. Y. J. Hu)

† Electronic Supplementary Information (ESI) available: Schematic setup for Ti^{3+} self−doped TiO_2 nanoparticles is shown in Fig. S1. The BET specific surface and pore size distribution of Ti^{3+} self–doped TiO_2 is shown in Fig. S2, XRD patterns of pristine TiO_2 and Ti^{3+} self–doped TiO_2 is shown in Fig. S3. HRTEM image of Ti^{3+} self-doped TiO_2 with mixture phase is shown in fig. S4. The photographs of different color of Ti^{3+} self–doped TiO_2 with different flow rate of hydrogen are shown in Fig. S5. TEM images of Ti^{3+} self–doped TiO_2 samples with different flow rate of carrier gas are in Fig. S6, XPS spectrum of O_{1s} is shown in Fig. S7, Photodegradation of MB in aqueous solutions using Ti^{3+} self–doped TiO_2, pristine TiO_2 and P25 as photocatalysts with irradiation of ultraviolet light is shown in fig. S8. UV−vis spectrum of MB aqueous solutions in different times by using Ti^{3+} self–doped TiO_2 as photocatalysts under the irradiation of visible light is shown in Fig. S9. See DOI: 10.1039/b000000x/

1 X. B. Chen, S. S. Mao, *Chem. Rev.* 2007, **107**, 2891.
2 M. Grätzel, *Nature* 2001, **414**, 338.
3 G. Liu, L. Z. Wang, H. G. Yang, H. M. Cheng, G. Q. Lu, *J. Mater. Chem.*, 2010, **20**, 831.
4 L. Sun, Z. L. Zhao, Y. C. Zhou, L. Liu, *Nanoscale*, 2012, **4**, 613.
5 P. Periyat, D. E. McCormack, S. J. Hinder, S. C. Pillai, *J. Phys. Chem. C*, 2009, **113**, 3246.
6 Y. Y. Wen, H. M. Ding, Y. K. Shan, *Nanoscale*, 2011, **3**, 4411.
7 K. Su, Z. Ai, L. Zhang, *J. Phys. Chem. C*, 2012, **116**, 17118.
8 Z.-R. Tang, Y. Zhang, Y.-J. Xu, *ACS Appl. Mater.Interfaces*, 2012, **4**, 1512.
9 N. Zhang, S. Liu, X. Fu, Y.-J. Xu, *J. Phys. Chem. C*, 2011,**115**, 9136.
10 X. Y. Pan, M.-Q. Yang, X. Z. Fu, N. Zhang, Y.-J. Xu, *Nanoscale*, 2013, **5**, 3601.
11 F. Zuo, L. Wang, T. Wu, Z. Y. Zhang, D. Borchardt, P. Y. Feng, *J. Am. Chem. Soc.*, 2010, **132**, 11856.
12 X. B. Chen, L. Liu, Y. P. Yu, S. S. Mao, *Science*, 2011, **331**,746.
13 G. H. Wang, Y. Ling, Y. Tang, X. Yang, R. C. Fitzmorris, C. Wang, J. Z. Zhang, Y. Li, *Nano Lett.*, 2011, **11**, 3026.
14 X. Y. Pan, M.-Q. Yang, X.Z. Fu, N. Zhang, Y.-J. Xu, *Nanoscale*, 2013, **5**, 3601.
15 L. R. Grabstanowicz, G. Shanmin, L. Tao, R. M. Rickard, T. Rajh, D.-J. Liu, *Inorg. Chem., 2013, 52, 3884.*
16 A. Naldoni, M. Allieta, S. Santangelo, M. Marelli, F. Fabbri, S. Cappelli, C. L. Bianchi, R. Psaro, V. Dal Santo, *J. Am.Chem. Soc.*, 2012, **134**, 7600.
17 K. Takeuchi, I. Nakamura, O. Matsumoto, S. Sugihara, M. Ando, T. Ihara, *Chem. Lett.*, 2000, **29**, 1354.
18 T. L. Thompson, J. T. Yates, *Chem. Rev.*, 2006, **106**, 4428.
19 L. Liu, C. Zhao, Y. Li, *J. Phys. Chem. C*, 2012, **116**, 7904.
20 R. Strobel, S.E. Pratsinis, *J. Mater. Chem.*, 2007, **17**, 4743.
21 J.C. Huo, Y.J. Hu, H. Jiang, W.J. Huang, Y.F. Li, W. Shao, C. Z. Li, *Ind. Eng. Chem. Res.*, 2013, **52**, 11029.
22 Y. J. Hu, C. Z. Li, F. Gu, Y. Zhao, *J. Alloys Compd.*, 2007, **432**, 5.
23 Hu, Y. J.; Xu, K. X.; Kong, L. Y.; Jiang, H.; Zhang, L.; Li, C. Z. *Chem. Eng. J.*, 2014, **242**, 220.
24 S. Y. Dhumal, T. L. Daulton, J. K. Jiang, B. Khomami, P. Biswas, *Appl. Catal. B-Environ.*, 2009, **86**, 145.
25 R. Strobel, S. E. Pratsinis, *Adv. Powder Technol.*, 2009, **20**, 190.
26 I. K. Herrmann, R. N. Grass, D. Mazunin, W. J. Stark, *Chem. Mater.*, 2009, **21**, 3275.
27 Y.F. Li, Y. J. Hu, J. C. Huo, H. Jiang, C. Z. Li, G. J. Huang, *Ind. Eng. Chem. Res.*, 2012, **51**, 11157.
28 X. D. Jiang, Y. P. Yang, J. Jiang, Y. S. Rong, Y. C. Wang, Y. C. Wu, C. X. Pan, *J. Phys. Chem. C.*, 2012, **116**, 22619.
29 K. Ming, Y. Z. Li, X. Cheng, T. T. Tian, P. F. Fang, F. Zheng, X. J. Zhao, *J. Am. Chem. Soc.*, 2011, **133**, 16414.
30 K. Suriye, P. Praserthdam, B. Jongsomjit, *Appl. Surf. Sci.*, 2007, **253**, 3849.

31 X. X. Zou, J. K. Liu, J. Su, F. Zuo, J. S. Chen, P.Y. Feng, *Chem. Eur. J.*, 2013, **19**, 2866.
32 M. S. Hamdy, R. Amrollahi, G. Mul, *ACS Catal.*, 2012, **2**, 2641.
33 T. Leshuk, R. Parviz, P. Everett, H. Krishnakumar, R. A. Varin, F. Gu, *ACS Appl. Mater. Interfaces*, 2013, **5**, 1892.
34 X. M. Yu, B. Kim, Y. K. Kim, *ACS Catal.*, 2013, **3**. 2479.